Setup for polarized neutron diffraction using a high-T_c superconducting magnet on the instrument POLI at MLZ and its applications

H Thoma[1], H Deng[2], G Roth[3], V Hutanu[2]

[1] Jülich Centre for Neutron Science JCNS at MLZ, Lichtenbergstr. 1, 85748 Garching, Germany
[2] Institute of Crystallography, RWTH Aachen University and Jülich Centre for Neutron Science (JCNS) at Heinz Maier-Leibnitz Zentrum (MLZ), Garching, Germany
[3] Institute of Crystallography, RWTH Aachen University, 52056 Aachen, Germany

E-mail: h.thoma@fz-juelich.de

Abstract. A new polarized neutron diffraction setup has been developed for the hot neutron single crystal diffractometer POLI at the Maier-Leibnitz Zentrum (MLZ) in Germany. This setup consists of a ^{3}He spin filter cell for polarization, a Mezei type double coil flipper optimized for short-wavelength neutrons, and a new high-T_c superconducting magnet producing fields up to 2.2 T. Because the magnet provides a symmetric field configuration, a dedicated guide field system was designed in order to avoid neutron depolarization in the zero-field node. The polarization transport efficiency of the whole setup was numerically simulated and optimized using COMSOL Multiphysics®. The polarization losses between the polarizer and the sample were confirmed to be smaller than 1.5% over the total field range of the magnet and the stray fields of the magnet did not affect the relaxation time T_1 of the ^{3}He spin filter polarizer. First experiments with antiferromagnetic and paramagnetic samples using the new setup have been successfully performed. Using the CCSL software, a reconstruction of the field induced spin density distribution in the weak ferromagnet $MnCO_3$ was performed in the paramagnetic state. Our results show the high performance and good resolution of the new setup.

1. Introduction

Polarized neutron diffraction (PND) is a powerful method to investigate magnetic structures. PND can be used for very precise magnetization measurements even for weak magnetic contributions. It allows the high-quality determination of magnetic form factors [1, 2], to untangle complex (e.g. chiral) magnetic structures, and to follow the movement of magnetic domains [3]. In this technique, spin flip measurements are carried out on a sample, located in a strong magnetic field. Optionally, the scattered beam can be analyzed to perform a polarization analysis along the given field direction at the sample.

Born in the late 1950s [4] and developed over subsequent decades by small groups of devoted experts, PND is nowadays a widespread, well established and recognized technique to answer difficult scientific questions about the detailed magnetic ordering in topical materials, often intractable with other methods. This has become possible because of sustained instrumental improvement and development, especially in the past two decades. Dedicated instruments have been developed, like D3 and D23 at the ILL (Institut Laue-Langevin, Grenoble, France) or 5C1

(VIP) and 6T2 at the LLB (Laboratoire Léon Brillouin, Gif sur Yvette, France), as well as other instruments at different neutron scattering facilities all over the world, and they provide this type of experiment to a broad user community [5-7].

One of the newest instruments of this type is the polarized single-crystal diffractometer POLI (**pol**arization **i**nvestigator) at the Maier-Leibnitz Zentrum (MLZ) in Germany. It has been successfully developed and built over the past few years [8, 9] and is the first instrument routinely using ^{3}He spin-filter cells (SFC) both to produce and to analyze neutron polarization [10] in combination with double-focusing non-polarized monochromators [11]. The spherical neutron polarimetry (SNP) setup, using the third-generation polarimeter device Cryopad [12], has been implemented on POLI as an initial experimental technique. Recently, POLI has been extended for two new polarized options, namely flipping ratio (FR) and uniaxial polarization analysis (PA), both for PND studies in applied magnetic fields provided by a new high-T_c superconducting magnet [13]. While in Ref. [13] we presented the novel magnet itself and its implementation, in the present report we concentrate mostly on the technical aspects of the setup, especially in regard to polarized neutrons, show detailed information about the development and optimization of the essential parts, and present new examples of its application.

2. Development of the new PND setup

The central device for the two options of the new PND setup at POLI, which are shown as an overview in Fig. 1, is the new high-T_c superconducting, cryogen-free magnet (Pos. 8 in Fig. 1), produced by the HTS-110 company in New Zealand [13]. The maximal field provided by the compact magnet in the center (sample, pos. 7 in Fig. 1) is of 2.2 T. As we discussed in

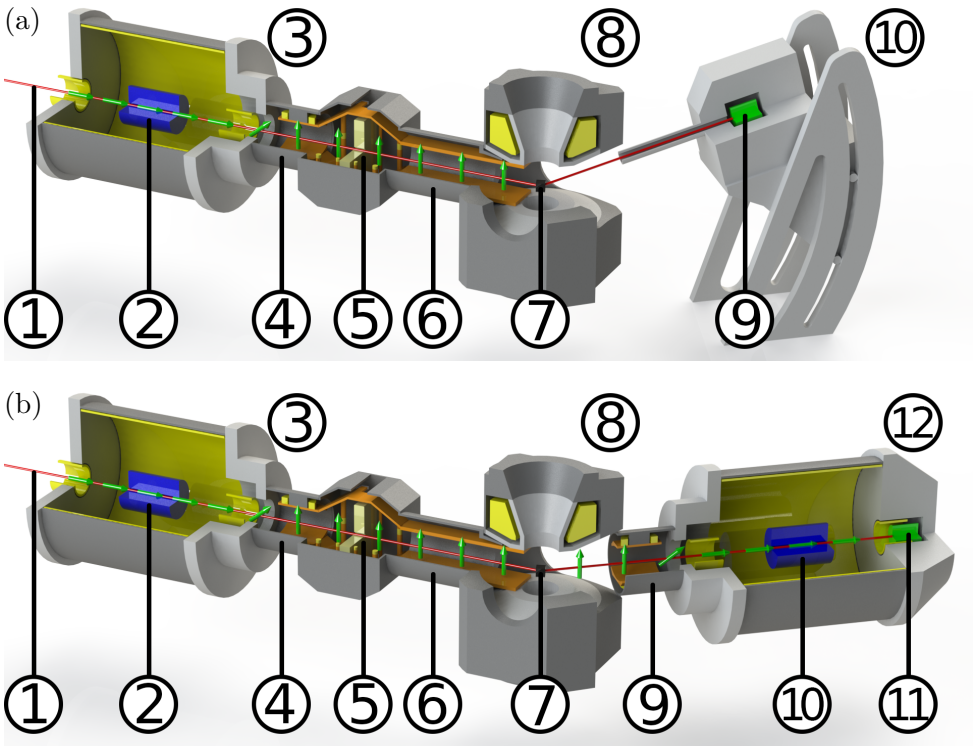

Figure 1. Setup components of the two new PND options at POLI with coils in yellow, guiding field pole pieces in orange, and magnetic yoke and shielding parts in dark gray. The field direction, and thus the polarization axis, is shown as green arrows. The notation of the numbered components are given in the main text.

detail in Ref. [13], the magnet has a large vertical and horizontal access, permitting access to out-of-plane Bragg reflections in the FR setup option by POLI's lifting mechanics (pos. 10 in Fig. 1a) for a single tube neutron detector (pos. 9 in Fig. 1a) and is passively shielded by a massive iron yoke (dark grey in Fig 1), reducing the stray field strength at a distance of one meter away from its center to about 10 Oe. But in contrast to usual magnets used for PND, the HTS magnet has a symmetrical design regarding its coils and iron yoke with respect to the horizontal plane. Thus, it has a zero field node in the beam path between the opposite directed main and fringe fields instead of an adiabatic field transition for the polarized neutrons, as usually realized for asymmetric magnets. This zero field node (or field reversal point), located 151 mm from the magnet's center, and thus close to its surface, must be removed in order to avoid beam depolarization. We realized this with a novel approach by introducing two optimized iron plates (orange parts of pos. 6 in Fig. 1) through the large openings of the magnet inside the yoke and connecting them to the magnet's poles close to its center, without touching the yoke. The development and optimization process by finite element simulations is described in more detail in the next section. In this way, the main field direction can be extracted to the outside of the magnet and directly coupled to a guide field. For the first time, the guide field is directed not along the stray field as usually for an asymmetric field geometry, but along the main field direction.

For polarization and analysis of the neutron beam in the new PND setup, the ^{3}He SFCs available from POLI's SNP setup are used [10]. Although the stray field of the HTS magnet is rather low due to the passive shielding by the yoke, its influence on the performance of the sensitive ^{3}He SFCs must be avoided. This issue could be in principle easily overcome by simply increasing the distance between the magnet and ^{3}He polarizer, because the stray field strength decays as the square of the distance from the magnet's center. However, on POLI the available experimental space is very limited. Therefore, a compromise between the maximal available distance of less than one meter and a proper shielding of the SFC is the only solution. We used a digital model to optimize the distance between the magnet and the polarizer and to estimate the possible field influence on the position of the SFC. The result showed, that due to the rather small fringe field strength outside the yoke and the 2 mm thick μ-metal shielding of the SFC (pos. 2 in Fig. 1) in the polarizer cavity (pos. 3 in Fig. 1), no significant depolarization of the ^{3}He inside the polarizer situated one meter away from magnet is expected. This was confirmed by first test experiments [13]. Directly after the polarizer, the neutron polarization is rotated vertically by an adiabatic field turn in the nutator (pos. 4 in Fig. 1).

To carry out PND measurements, a non-adiabatic spin transition for a spin flip needs to be provided between the vertical guide field in the nutator and the guide field, extracted by the pole pieces from the main field in the magnet. Although a cryoflipper [14], a radio frequency (RF) flipper, and even an adiabatic fast passage (AFP) flipper [15] were considered, we decided to use a Mezei type double coil flipper [16], since it is cheap in realization and operation, has a simple and robust design, and is quite compact in the beam direction. The beam attenuation occurring on the windings of the Mezei coil placed in the beam path is not significant for the short wavelength neutrons used at POLI (about 1.4% at a wavelength of 0.9 Å). Also a change of the flipping efficiency in dependence on external fringe fields of the magnet is more relaxed in our case, since the fringe fields of the new HTS magnet are significantly weaker than for typical superconducting magnets without iron yoke. The design of the new flipper has been optimized by detailed numerical simulations and is addressed in Sec. 4.

For the PA option shown in Fig. 1b, an analyzer is added for the scattered beam. This type of setup, first described and used by *Moon et al.* [17], allows to measure changes of the neutron polarization by the scattering process and to distinguish between nuclear and magnetic scattering contributions. For the new PND setup, the second SFC analyzer (pos. 10 in 1b) is integrated together with a point-detector (pos. 11 in 1b) into the Decpol [9] (pos. 12 in 1b), a

standard device from the SNP setup. This Decpol is equipped with a second nutator (pos. 9 in 1b) to turn the polarization adiabatically back along the beam direction. Compared to the lifting counter from the FR option, the Decpol is limited only to the instrumental plane.

In first measurements, the polarized neutron spin transport efficiency of the new PND setup at POLI, accounting for all setup-related losses and the flipping efficiency, was confirmed to be around 99% for the complete field range of the HTS magnet in the FR option, and up to 1.2 T in the PA option [13].

3. Development of the guide field segment

For the development and optimization of the guide field segment (pos. 6 in Fig. 1), the precise knowledge of the HTS magnet's field distribution is mandatory. Thus, the magnet was modeled using the COMSOL Multiphysics® software package (https://www.comsol.com/) and its material properties adjusted such, that the simulated field distribution values reproduce well the measured ones [13]. It turned out, that the yoke's material can be well described with the *soft iron* material provided by COMSOL. In a next step, a first draft of the guiding field plates was set

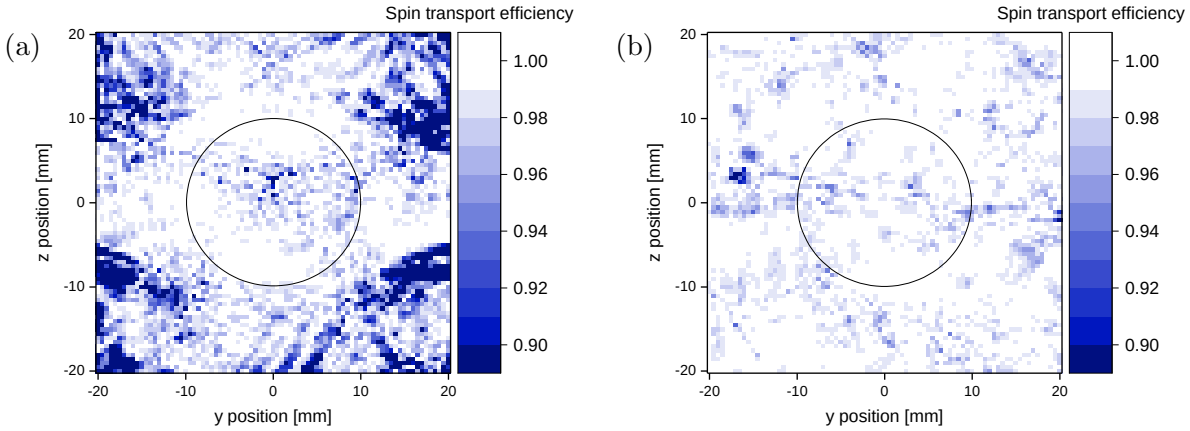

Figure 2. Simulated polarized neutron spin transport efficiency over the complete beam profile for a wavelength of 1.15 Å and a field of 2.1 T. The z position is vertical, the y position lateral to the beam. This was calculated using a 81 × 81 grid. The black circle has a diameter of 20 mm. The mean value of the spin transport efficiency inside this circle was used as a parameter for the comparison between different geometries of the polar plates: a) denoted as geometry three and b) as geometry two in Fig. 3.

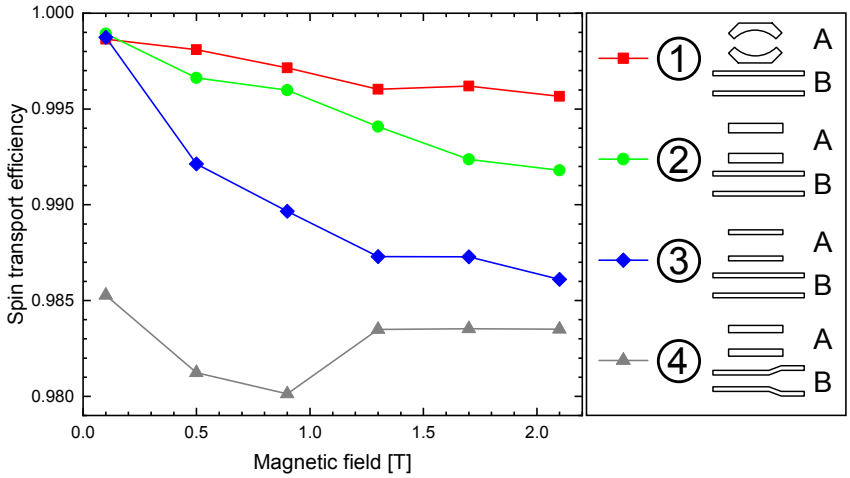

Figure 3. Simulated spin transport efficiency as function of the main field in the magnet for different geometries of the guide field's polar pieces and a wavelength of 1.15 Å. The A view shows the cross section of the pole pieces in the plane normal to the beam. The B view shows the shape along the beam.

up and their performance simulated in the field of the HTS magnet. In an iterative process, this draft was optimized regarding several aspects including the length, shape, and thickness of the pole pieces. Using COMSOL's LiveLink^{TM} for MATLAB® (https:// www.comsol.com/livelink-for-matlab), the simulated field map was read out directly and forwarded to a bespoke C-program, which calculated the expected spin transport efficiency for the complete beam profile based on the simulated field data. Two exemplary beam polarization profiles are shown in Fig. 2. To calculate these distributions, the Larmor precession of the polarization vector was simulated for each y-z grid point in the beam profile for a neutron path from the ^{3}He SFC (pos. 2 in Fig. 1) to the sample (pos. 7 in Fig. 1). The average polarization transport efficiency over this profile served finally as reference for the comparison between the different designs or geometries of the polar pieces. Since the whole simulation procedure was fully controlled by a MATLAB® script (https://www.mathworks.com/) and the quality of each design could be reduced to a single parameter, namely the spin transport efficiency, the optimization process of individual components could be almost completely automatized. As example, a typical comparison of four different shapes of pole pieces during the optimization process is shown in Fig. 3. Cases two and three differ only in their thickness, whereas case one uses curved poles with optimized shape and case four has an inclined part along the beam direction to reduce the influence of the stray fields. Case two, showing a negligible small reduction of the efficiency at higher fields, however being much easier and cheaper in the production as case one, has been used in the final design. Experimentally, we observe an overall spin transport efficiency of 98.5% for the complete setup, which is only slightly lower than the simulated value. The difference between calculated and experimentally measured spin transport efficiency can be easily accounted by the finite flipping efficiency, imperfect surfaces, screws, and remanent magnetization not included in the idealized simulation. Additionally, the simulations with COMSOL showed, that a shielding for the pole pieces by an iron cylinder (dark gray part of pos. 6 in Fig. 1) is necessary to withstand the maximal stray field of around 650 Oe close to the zero field node at maximal magnet power.

4. Optimization of the Mezei type double coil spin flipper

The design of the new flipper, shown as photograph in Fig 4, has been optimized by detailed numerical simulations for several aspects of POLI. The size (height and width) of the flipper has been adjusted to ensure a homogeneous flip-field over the large beam cross section. The length of the flipper in the beam path was adjusted to limit the necessary flipping coil current to 4 A at the shortest available wavelength at POLI of 0.55 Å. Since simulation and test experiments showed, that the heating provided by 4 A could be critical for long-time measurements, an additional air pressure cooling system (pos. 3 in Fig. 4) was adopted. To ensure a maximal independence from the HTS magnet's main field, to minimize variations in the compensation coil current, and to guarantee a stable flipping efficiency, the new Mezei type double coil flipper (pos. 5 in Fig. 1) is located in a homogeneous guide field, created by inclined polar pieces (orange plates in

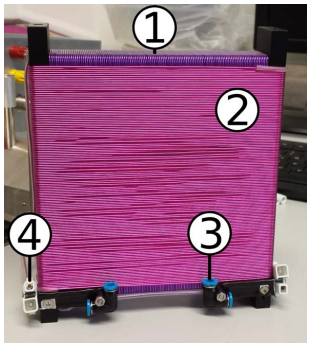

Figure 4. Photograph of the Mezei type double-coil flipper (pos. 5 in Fig. 1) without guiding field and shielding. Visible are: (1) The flipping coil, generating a magnetic field perpendicular to the polarization direction, which causes a neutron spin rotation of 180° (a so called pi-flip); (2) the compensation coil, which is used to suppress the external guide field; (3) the two L-shaped connectors at the bottom used for pressure air blowing for cooling (another two on the backside of the flipper); (4) the electrical connectors for the coils on the side.

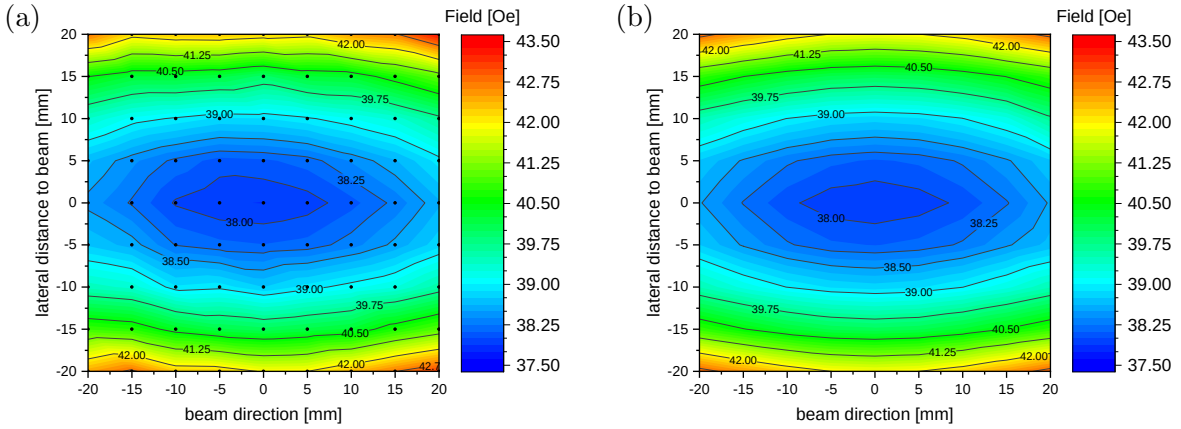

Figure 5. (a) Measured and (b) with COMSOL simulated vertical field strength distribution in the horizontal plane of the flipper's guide field, generated by permanent magnets. The black dots in (a) mark the measured positions. The Meizei flipper is placed such, that its center corresponds to the (0,0) position in the graph.

pos. 5 in Fig. 1) and driven by small Nd-based permanent magnets (yellow small cylinders in the front plane of pos. 5 in Fig. 1). The guide field in the flipper, as well as the entire flipper construction, were optimized using a COMSOL software model. The comparison between the measured and simulated guide field strength in the horizontal plane at the flipper position is shown in Fig. 5, and an almost perfect agreement is observed. Due to the close vicinity (0.5 m) to the HTS magnet, this guide field construction is then additionally shielded by an iron box (dark gray parts from pos. 5 in Fig. 1). The new Mezei flipper was calibrated and its high flipping efficiency experimentally proven at different wavelengths and all available fields in the magnet (supplementary materials in Ref. [13] for more details). .

5. Field induced magnetization density in paramagnetic $MnCO_3$

One of the major strengths of PND in applied magnetic fields is the reconstruction of magnetization density maps in the unit cell. Usually, the spatial distribution of magnetic moments is accounted by the magnetic form factor, which can be approximated by an empirical model provided by *Brown* [18]. In the simplest case, for an orbital quantum number $L = 0$, a spherical distribution is assumed. However, in some cases (e.g. due to interactions in ordered materials or anisotropies) the expected distribution can be distorted. Thus, it would be of interest, to visualize these non-ideal magnetic moment distributions, especially for molecules, but also for other magnetic compounds. Since the magnetic scattering factor $\boldsymbol{M}$ is nothing else than the Fourier transform (FT) of the magnetization density $\boldsymbol{m}(\boldsymbol{r})$ in the unit cell for a specific scattering vector $\boldsymbol{q}$, $\boldsymbol{m}(\boldsymbol{r})$ can be obtained by an inverse FT [19]. Although PND conserves, in contrast to unpolarized measurements, some required phase information in the nuclear magnetic interference term, it does not measure $\boldsymbol{M}$ directly, only its projections on certain directions [20]. Therefore, the additional assumption of $\boldsymbol{M}$ pointing along the applied field direction must be made, in order to determine the Fourier component $M(\boldsymbol{q})$ from a FR measurement. This assumption is reasonable for example for paramagnetic materials, but in ordered or frustrated systems, this must not be fulfilled.

To calculate the spin density map from the measured Fourier components $M(\boldsymbol{q})$, different methods are available. The first one is the direct inverse FT. This method is very simple and fast, but to reconstruct $m(\boldsymbol{r})$ perfectly, all reflections from the complete reciprocal space should be measured exactly. This is not possible, since data collections are always restricted by the instrumental geometry and polluted by noise. As result, the magnetization density observed

from the direct inverse FT often shows heavy truncation and noise effects [19]. A possible solution to suppress these artifacts is the maximum entropy method (MEM). Compared to the direct inverse FT which assumes not measured Fourier component to be zero, they are not considered for reconstruction in MEM. Furthermore, by a compromise between a good fit to the data and the highest possible entropy for the reconstruction, a very smooth and clear magnetization density distribution is observed. A tool for the maximum entropy reconstruction of FR measurements is for example given by the MEND [21] subroutine of CCSL [22].

As one of the first measurements with the FR option of the new PND setup at POLI, we studied field induced ferromagnetic magnetization in a rhodochrosite ($MnCO_3$) single crystal. $MnCO_3$ crystalizes in the rhombohedral symmetry $R\bar{3}c$ and undergoes an antiferromagnetic transition at $T_N = 32.43\,K$ [23]. A missing centrosymmetry between neighboring Mn atoms allows the presence of the Dzyaloshinskii-Moriya interaction and the resulting magnetic order is slightly canted, presenting the so called weak ferromagnetism. This low temperature phase of $MnCO_3$ was studied by *Brown et al.* [24] with polarized neutrons and recently by *Beutier et al.* [25] with magnetic resonant X-ray scattering. In our experiment, we focus on the paramagnetic state of $MnCO_3$ and use a temperature of 64 K, which is about double as high as the T_N. The sample was oriented in the way that the field of 2.2 T was applied along the a-axis. Using the lifting counter and a short neutron wavelength of 0.9 Å, asymmetry values for a set of 214 Bragg reflections were collected. Fixing the total induced magnetization for the complete hexagonal unit cell to $0.78\,\mu_B$, as observed in magnetization measurements by *Borovik-Romanov et al.* [26], the MEND subroutine of CCSL was used to reconstruct the maximum entropy solution shown in Fig. 6. The observed magnetization ellipsoids in Fig. 6a are clearly located at the Mn positions. The elongation of these ellipsoids along the field direction can be attributed to the reduced instrumental resolution for this vertical direction, which is only generated by the out of plane reflections. The projection of this 3D magnetization density to the instrumental plane, thus the plane perpendicular to the a-axis, which is formed by the c-axis and the [120] direction, is shown in Fig. 6b. The resulting 2D in plane magnetization distribution around the Mn position is slightly elongated along the [001] direction. Worth mentioning, that the direction of the observed non-spherical distortion coincides with that of the weak ferromagnetism occurring in the antiferromagnetic phase of $MnCO_3$ due to the Dzyaloshinskii-Moriya interaction. Remarkable is also the smooth background of the density obtained by the maximum entropy solution, showing no truncation or noise effects.

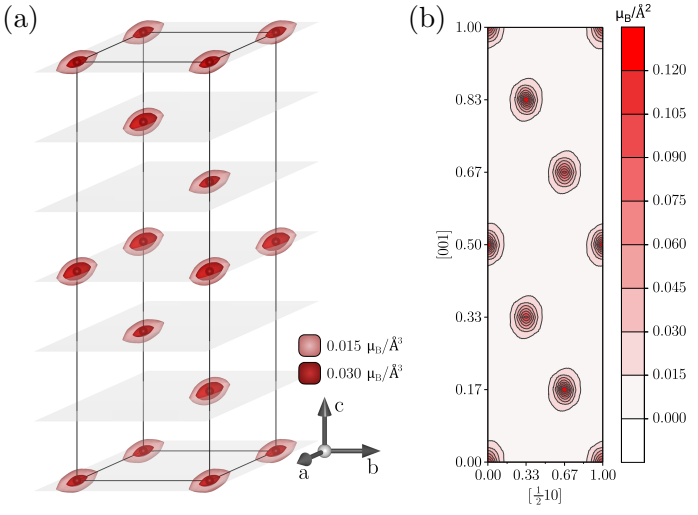

Figure 6. Magnetization density distribution in the unit cell of rhodochrosite ($MnCO_3$) at 64 K and applied magnetic field of 2.2 T along [100] direction, reconstructed with MEND subroutine of CCSL from the measured asymmetries on 214 Bragg reflections using new PND setup on POLI. (a) 3D magnetization density distribution in the hexagonal unit cell. The density ellipsoids located at the Mn atom positions (black spheres) are elongated along the field direction. (b) Magnetization density projected on the instrumental plane by integration along the field direction.

6. Conclusions

A new compact 2.2 T magnet made of high-T_c superconductor with symmetric field configuration has been employed for the development of the PND setup on POLI. For this setup, the magnet has been combined with an existing ^{3}He polarizer, a newly developed Mezei type double coil flipper, and a special guide field segment, which is inserted into the magnet. All parts of the new setup were carefully designed and optimized for the given special conditions at POLI using COMSOL Multiphysics® software in combination with MATLAB® Livelink software tool. Both available PND options, namely FR and uniaxial PA, were calibrated and tested, showing a high polarization transport efficiency of around 99% for all available field strengths [13].

High quality 2D and 3D maps of the field induced magnetization density distribution in the unit cell of the Dzyaloshinskii-Moriya antiferromagnet $MnCO_3$ at 64 K in the paramagnetic state were obtained using the measurement of 214 asymmetries of accessible Bragg reflections on POLI for a neutron wavelength of 0.9 Å. The maximal entropy reconstruction was applied. The obtained results clearly demonstrate the high performance of new PND setup in combination with the good resolution at POLI, and opens it for the usage by the wide user community.

7. Acknowledgments

We would like to thank W. Luberstetter for the technical support in realization of the new PND setup, S. Masalovich for providing us with polarized ^{3}He for tests and experiments and V. Dmitrienko for borrowing us a single crystal of rhodochrosite. The instrument POLI is operated by RWTH Aachen and FZ Jülich (Jülich Aachen Research Alliance JARA).

References

[1] Wilkinson C, Keen D A, Brown P J and Forsyth J B 1989 *J. Phys. Condens. Matter* **1** 3833–3839
[2] Lebech B, Rainford B, Brown P and Wedgwood F 1979 *J. Magn. Magn. Mater.* **14** 298–300
[3] Nathans R, Pickart S J, Alperin H A and Brown P J 1964 *Phys. Rev.* **136** A1641–A1647
[4] Nathans R, Shull C G, Shirane G and Andresen A 1959 *J. Phys. Chem. Solids* **10** 138–146
[5] Lelièvre-Berna E, Bourgeat-Lami E, Gibert Y *et al.* 2005 *Phys. B Condens. Matter* **356** 141–145
[6] Gukasov A, Goujon A, Meuriot J L, Person C, Exil G and Koskas G 2007 *Phys. B Condens. Matter* **397** 131–134
[7] Gukasov A, Rodrigues S, Meuriot J L, Robillard T, Sazonov A, Gillon B, Laverdunt A, Prunes F and Coneggo F 2013 *Phys. Procedia* **42** 150–153
[8] Hutanu V, Meven M and Heger G 2007 *Phys. B Condens. Matter* **397** 135–137
[9] Hutanu V, Meven M, Lelièvre-Berna E and Heger G 2009 *Phys. B Condens. Matter* **404** 2633–2636
[10] Hutanu V, Meven M, Masalovich S, Heger G and Roth G 2011 *J. Phys. Conf. Ser.* **294** 012012
[11] Hutanu V 2015 *J. Large-scale Res. Facil. JLSRF* **1** A16
[12] Hutanu V, Luberstetter W, Bourgeat-Lami E, Meven M, Sazonov A, Steffen A, Heger G, Roth G and Lelièvre-Berna E 2016 *Rev. Sci. Instrum.* **87** 105108
[13] Thoma H, Luberstetter W, Peters J and Hutanu V 2018 *J. Appl. Crystallogr.* **51** 17–26
[14] Tasset F 1989 *Phys. B Condens. Matter* **156-157** 627–630
[15] Babcock E, Petoukhov A, Chastagnier J *et al.* 2007 *Phys. B Condens. Matter* **397** 172–175
[16] Mezei F 1972 *Zeitschrift für Phys. A Hadron. Nucl.* **255** 146–160
[17] Moon R M, Riste T and Koehler W C 1969 *Phys. Rev.* **181** 920–931
[18] Brown P J 2006 *Int. Tables Crystallogr. Vol. C Math. Phys. Chem. tables* ed Prince E (Chichester: Wiley) chap 4.4.5., pp 454–461
[19] Papoular R J and Gillon B 1990 *Europhys. Lett.* **13** 429–434
[20] Williams W G 1988 *Polarized Neutrons* Oxford science publications (Oxford: Clarendon Press)
[21] Sakata M, Uno T, Takata M and Howard C J 1993 *J. Appl. Crystallogr.* **26** 159–165
[22] Matthewman J C, Thompson P and Brown P J 1982 *J. Appl. Crystallogr.* **15** 167–173
[23] Borovik-Romanov A S 1959 *Sov. Phys. Jetp-Ussr* **9** 539–549
[24] Brown P J and Forsyth J B 1967 *Proc. Phys. Soc.* **92** 125–135
[25] Beutier G, Collins S P, Dimitrova O V *et al.* 2017 *Phys. Rev. Lett.* **119** 167201
[26] Borovik-Romanov A S and Orlova M P 1957 *Sov. Phys. - JETP* **4** 531–534